Energy Transfer in Reconnection and Turbulence

S. Adhikari[1],*, T.N. Parashar[2,1], M.A. Shay[1,3], W.H. Matthaeus[1,3],
P. S. Pyakurel[4], S. Fordin[1], J.E. Stawarz[5], and J.P. Eastwood[5]

[1]*Department of Physics and Astronomy, University of Delaware, Newark, Delaware 19716, USA*
[2] *School of Chemical and Physical Sciences, Victoria University of Wellington, Wellington 6012, NZ*
[3] *Bartol Research Institute, Department of Physics and Astronomy,*
University of Delaware, Newark, Delaware 19716, USA
[4] *Space Sciences Laboratory, University of California, Berkeley, CA 94720, USA and*
[5] *Department of Physics, Imperial College London, SW7 2AZ, UK*
(Dated: December 3, 2021)

Reconnection and turbulence are two of the most commonly observed dynamical processes in plasmas, but their relationship is still not fully understood. Using 2.5D kinetic particle-in-cell simulations of both strong turbulence and reconnection, we compare the cross-scale transfer of energy in the two systems by analyzing the generalization of the von Kármán Howarth equations for Hall magnetohydrodynamics, a formulation that subsumes the third-order law for steady energy transfer rates. Even though the large scale features are quite different, the finding is that the decomposition of the energy transfer is structurally very similar in the two cases. In the reconnection case, the time evolution of the energy transfer also exhibits a correlation with the reconnection rate. These results provide explicit evidence that reconnection dynamics fundamentally involves turbulence-like energy transfer.

Introduction: Many naturally occurring and man-made plasmas are observed to be in a turbulent state [1–6] driven at large scales, either externally or by an energy reservoir. Nonlinear couplings subsequently transfer energy from large scales to smaller kinetic scales. Magnetic reconnection [7, 8], frequently observed in these systems, is itself a nonlinear process, though largely studied independently of turbulence. In many cases, turbulence is either a consequence or driver of the reconnection process [7, 9–11]. In recent literature, one finds numerous studies of the properties of reconnection that emerge in a turbulent environment in both three dimensions [12, 13] and two dimensions [14]. Such studies often focus on spectra, dimensionality and reconnection rates [15, 16] or on more subtle issues such as violations of flux freezing [17, 18] in turbulence with implication for reconnection. Similar characterizations apply to studies of turbulence properties, typically spectral and correlation properties [19, 20] that emerge in standard reconnection. Reconnection is also studied as a process subsidiary to turbulence, either by diagnosing reconnection occurring in turbulence [7, 11, 21–23] or studying how reconnection modifies small scale energy transfer [24–31]. Turbulence also emerges in association with reconnection-related instabilities [20, 24, 32–35]. To our knowledge previous works have not directly examined energy transfer in a standard reconnection problem, nor have they compared such transfer to that of homogeneous turbulence.

Recent kinetic particle-in-cell (PIC) simulations show that laminar reconnection in 2D and 3D exhibits a Kolmogorov $-5/3$ magnetic spectrum [19, 20, 33, 36], raising intriguing questions: "How do the properties of energy transfer in reconnection and turbulence compare? Does the similarity of their spectra indicate a similarity of spectral transfer in the two cases?" Here we examine the properties of energy transfer in reconnection and turbulence by a parallel analysis of energy transfer budgets employing the von Kármán Howarth equations generalized to Hall-MHD [37, 38], and written in terms of structure functions. This formulation encompasses the famous MHD cascade law [37] including the Hall effect [38–40]. The analysis employs 2.5D kinetic PIC simulations of both strong turbulence and laminar reconnection, each initialized in a regime expected to be close to incompressibility. Details of energy transfer in both simulations are found to be structurally very similar, with majority of the energy transfer occurring through incompressive channels. This provides evidence that reconnection dynamics involves energy transfer akin to standard turbulence. Consistent with this, we find that the time evolution of the energy transfer correlates with the reconnection rate. Since cross scale coupling is arguably the defining characteristic of turbulence [41], we find an even greater similarity of reconnection and turbulence than has been previously reported.

Simulations: To study the energy transfer in reconnection, we use two fully-kinetic 2.5D PIC simulations - a strong turbulence case (Simulation A) and a laminar reconnection case (Simulation B); see Table I. Time is normalized to the inverse ion cyclotron frequency ($w_{ci} = (eB_0/m_i c)$), where B_0 is the normalizing magnetic field. Length is normalized to the ion inertial length $d_i = \sqrt{c^2 m_i/(4\pi n_0 e^2)}$, where n_0 is the normalizing number density. Speed is normalized to the ion Alfvén speed ($v_A = d_i \omega_{ci}$) and temperature to $T_0 = m_i v_A^2$. Following standard turbulence notation [2, 42, 43] magnetic field ($\mathbf{b} \equiv \mathbf{B}/\sqrt{4\pi m_i n_0}$) and current ($\mathbf{j} \equiv \mathbf{J}/ne$) are normalized to v_A.

The undriven turbulence simulation is initialized with

* subash@udel.edu

TABLE I. Simulation details: Size of the simulation (L_{box}), grid spacing (Δx), guide field (B_g), temperature (T), mass (m), ions/electrons (i/e), the root mean square value (rms) $\delta b_{rms} = \sqrt{\langle |\mathbf{b} - \langle \mathbf{b} \rangle_r|^2 \rangle_r}$, and the fluctuation (turbulence) amplitude $\delta Z = \sqrt{(\delta b_{rms})^2 + (\delta u_{rms})^2}$.

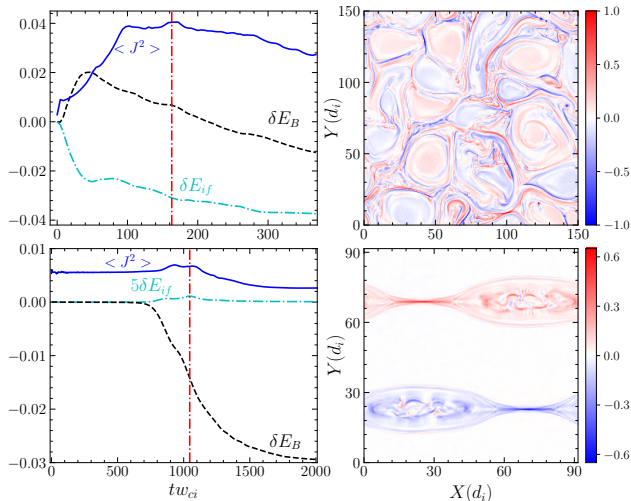| Run	Type	$L_{box}[d_i]$	grids	$\Delta x[d_i]$	B_g	T_i/T_e	m_i/m_e	n_b	δb_{rms}	δu_{rms}	δZ
A	Turbulence	149.6	4096^2	0.036	1	0.3/0.3	25	1	$1/\sqrt{10}$	$1/\sqrt{10}$	$1/\sqrt{5}$
B	Reconnection	91.59	4096^2	0.022	0	0.05/0.01	25	1	$1/\sqrt{5}$	0	$1/\sqrt{5}$

FIG. 1. Left panel: Evolution of the mean square current (solid), change in magnetic (δE_B) (dashed), and ion-flow (δE_{if}) energy per unit mass (dash-dot) for simulations A (top) and B (bottom); the vertical line denotes: (sim A) maximum rms J at $t\omega_{ci} = 163$ or (sim B) late quasi-steady reconnection at $t\omega_{ci} = 1045.6$. Right panel: J_z of simulation A (top) and B (bottom).

Fourier modes $k \in [2,4] \times \frac{2\pi}{149.6}$ with average wave number $k_{av} \approx 3 \frac{2\pi}{149.6} = 0.126$; see [44]. The reconnection simulation is initialized with a double Harris current sheet (with $k_{av} \approx 2\pi/91.59 = 0.068$). Reconnection is triggered by a small magnetic perturbation; see [36]. To facilitate comparison, simulation B normalization values are modified from [36] as $B_0 \to \frac{1}{\sqrt{5}} B_0$ and $n_0 \to 5 n_0$. With this modification simulations A and B have the same background density n_b and the same initial fluctuation amplitude δZ, as defined in Table I.

Fig. 1 provides an overview. In the turbulence simulation A, an initial Alfvénic exchange of energy occurs between the ion-flow and magnetic field. The fluctuation energy ($E_{if} + E_B$) decreases monotonically, as electrons and ions are heated [44]. For simulation B, E_B decreases, as reconnection transfers most of the energy to thermal energy and a small fraction to E_{if}. The mean square current peaks during the quasi-steady phase of reconnection and falls as δE_B decreases. The energy decay rate becomes significant after reconnection onset, and peaks during the late quasi-steady phase ($tw_{ci} = 1045.6$). The energetics and the currents have a very different evolution

in the two cases. On this basis one might expect that reconnection and turbulence would both exhibit dissimilar inertial ranges when energy transfer is quantified.

Energy transfer rate: To quantify the energy transfer rates in the simulation, we employ a form of the Hall-MHD von Kármán Howarth equation, which for steady state high Reynolds numbers reduces to the third-order cascade law [37]. Formally appropriate for incompressible MHD, this representation is expected to be a good approximation in weakly compressive MHD [45] and kinetic plasma [46] turbulence, understanding that at sub-proton scales, non-MHD effects dominate. In isotropic hydrodynamic turbulence, the third-order law gives an exact relationship between energy decay rate and a third-order structure function [47]. Hellinger et. al. [38] examined the decomposition of the MHD von-Kármán Howarth equations [37] for Hall-MHD, which will be referred as the Hellinger formulation.

Following standard theory [48], the von Kármán Howarth equations may be rewritten in terms of increments $\delta \mathbf{u}(\mathbf{r},l) \equiv \mathbf{u}(\mathbf{r}+l) - \mathbf{u}(\mathbf{r})$ and $\delta \mathbf{b}(\mathbf{r},l) \equiv \mathbf{b}(\mathbf{r}+l) - \mathbf{b}(\mathbf{r})$, where $\mathbf{r}$ is a vector in real space and l is the spatial lag, corresponding roughly to the inverse spectral wavenumber $\mathbf{k}/k^2$. Second-order structure functions are mean square values of these increments, e.g. $S_u(l) = \langle |\delta \mathbf{u}(\mathbf{r},l)|^2 \rangle_r$, where $\langle \dots \rangle_r$ is a spatial average over $\mathbf{r}$. Typically, structure functions are averaged over lag directions, giving $\overline{S_u(l)} \equiv \langle \langle |\delta \mathbf{u}(\mathbf{r},l)|^2 \rangle_r \rangle_{\Omega_l}$, where $\langle \dots \rangle_{\Omega_l}$ denotes averaging over solid angle [49]. Physically, $\frac{1}{4} S(l) = \frac{1}{4} \overline{S(l)} = \frac{1}{4} (\overline{S_u(l)} + \overline{S_b(l)})$ is the energy (flow + magnetic) inside a lag space sphere of radius $l = |l|$.

To study the energy transfer we employ the Hellinger formulation hereafter called simply the "third-order law" for convenience [38, 50, 51]:

$$\frac{1}{4} \frac{\partial S(l)}{\partial t} + \frac{1}{4} \nabla_l \cdot \mathbf{Y}(l) + \frac{1}{8} \nabla_l \cdot \mathbf{H}(l) = \frac{1}{2} D(l) - \epsilon, \quad (1)$$

where ∇_l is the lag space gradient. The MHD transfer term [37] $\mathbf{Y}(l) = \langle \delta \mathbf{u}|\delta \mathbf{u}|^2 + \delta \mathbf{u}|\delta \mathbf{b}|^2 - 2\delta \mathbf{b}(\delta \mathbf{u} \cdot \delta \mathbf{b}) \rangle_r$ and the Hall transfer term [38] is $\mathbf{H}(l) = \langle 2\delta \mathbf{b}(\delta \mathbf{b} \cdot \delta \mathbf{j}) - \delta \mathbf{j}|\delta \mathbf{b}|^2 \rangle_r$ are mixed third-order structure functions generalizing the hydrodynamic Yaglom flux [52]. Similarly, ϵ is the total dissipation rate and $D(l)$ is a lag dependent dissipation term that vanishes (by definition) outside the dissipation range. These are both normalized to $\omega_{ci} v_A^2$. In collisionless plasma simulations [53], the

exact functional of these terms are not known. In a system with kinematic viscosity ν and resistivity η, dissipation is explicitly $\epsilon = \nu\langle(\nabla\mathbf{u}:\nabla\mathbf{u})\rangle_r + \eta\langle\nabla\mathbf{b}:\nabla\mathbf{b}\rangle_r$ and $D(\boldsymbol{l}) = \nu\nabla_l^2 S_u(\boldsymbol{l}) + \eta\nabla_l^2 S_b(\boldsymbol{l})$.

Physically, the second and third terms in Eq. 1 are the energy transfer rates through the surface of a lag sphere of radius l due to the MHD and Hall nonlinearities, respectively; positive (negative) is out of (into) the spherical surface.

In adopting Eq. 1 as the basis for our comparison of turbulence and reconnection, we choose to focus on incompressive energy transfer, which underlies the most basic Sweet Parker reconnection analysis, while providing the baseline theory of turbulence as applied to systems such as the solar wind. With these approximations, Eq. 1 is a complete description of energy transfer and does not involve the involve the issue of locality or nonlocality (e.g., [54]). We note that recent progress has developed Yaglom-like relations for compressible (Hall) MHD [39, 40, 55, 56]. However, we opt to work with incompressible form represented by Eq. 1, a choice partially justified when we find below that incompressive channels account for the majority of energy transfer. Further study including the compressive transfer channels is deferred to a later study.

To study the energy transfer, we compare the left-hand side terms in Eq. 1 calculated from the simulations. For each time, the second and third-order structure functions are calculated as a function of lag vector (l_x, l_y) at each spatial grid point[49]. The divergence is computed in lag space, and 1D forms are obtained using the angle averaging technique [57], yielding omni-directional estimates $\overline{S(\boldsymbol{l})}$, $\overline{\nabla_l \cdot \mathbf{Y}(\boldsymbol{l})}$, and $\overline{\nabla_l \cdot \mathbf{H}(\boldsymbol{l})}$. Therefore, the 1D form of the Hellinger formulation can be written as:

$$\frac{1}{4}\overline{\frac{\partial S(\boldsymbol{l})}{\partial t}} + \frac{1}{4}\overline{\nabla_l \cdot \mathbf{Y}(\boldsymbol{l})} + \frac{1}{8}\overline{\nabla_l \cdot \mathbf{H}(\boldsymbol{l})} = \frac{1}{2}\overline{D(\boldsymbol{l})} - \epsilon, \quad (2)$$

We emphasize that each term in Eq. 2 is averaged over direction in lag-space and is therefore exact even for non-isotropic systems [57]. Furthermore, because of the periodicity of the simulations, each term in Eq. 2 is independent of position, i.e. the simulations are effectively homogeneous.

For both simulations, the terms of Eq. 2 are time-averaged over an interval ($\Delta t\omega_{ci}$) centered on the vertical red lines in Fig. 1 (sim A: $\Delta t\omega_{ci} \approx 20$; sim B: $\Delta t\omega_{ci} = 22.4$). The average rate of change of $S(l)$ over this interval is $\partial S(l)/\partial t$. The average rate of change of $E_B + E_{if}$ from Fig. 1 gives an estimate $\epsilon^* = \partial(E_B + E_{if})/\partial t$ for the decay rate. $\overline{\nabla_l \cdot \mathbf{Y}(\boldsymbol{l})}$, and $\overline{\nabla_l \cdot \mathbf{H}(\boldsymbol{l})}$ are averaged over 5 (sim A) and 3 (sim B) evenly spaced times in this interval.

The results are shown in Fig. 2. For the turbulence run (left panels), the energy containing range and the inertial range are dominated by $\overline{\partial S(\boldsymbol{l})/\partial t}$ and $\overline{\nabla_l \cdot \mathbf{Y}(\boldsymbol{l})}$, respectively. In the "kinetic/Hall" range the Hall term $\overline{\nabla_l \cdot \mathbf{H}(\boldsymbol{l})}$ is $\gtrsim$ the other terms. Notably, at large length

scales ($l \gtrsim d_i$), the sum of the terms are constant and approximately equal to ϵ^*. Constancy of the energy transfer rate suggests the existence of quasi-steady energy cascade [58]. $S(l)$ in Fig. 2 exhibits an approximate slope of $2/3$ for the range of lags where the sum of the terms is constant. The results are consistent with similar analysis in hybrid simulations [38]. At late times when the mean square current decreases ($t\omega_{ci} \gtrsim 250$), all the contributions diminish (not shown). However, the region of dominance of each term persists, resulting in a roughly constant MHD scale transfer. Similar to the abbreviated "inertial range" seen in Fig 2, it is not unusual for simulations evaluating the Yaglom law to find a very limited range of applicability, due to limited scale separation; see e.g, [51, 57]).

The reconnection simulation (Fig. 2 (middle and right)) exhibits results similar to the turbulence simulation. In the energy containing range $\overline{\partial S(\boldsymbol{l})/\partial t}$ dominates and is roughly constant, while the MHD energy transfer term $\overline{\nabla_l \cdot \mathbf{Y}(\boldsymbol{l})}$ dominates and flattens in the inertial range; $\overline{\nabla_l \cdot \mathbf{H}(\boldsymbol{l})}$ becomes significant approaching the kinetic range. Reconnection displays a wide inertial range during the early quasi-steady phase $t\omega_{ci} = 824.3$ (middle panel in Fig. 2), where the Yaglom flux term ($\overline{\nabla_l \cdot \mathbf{Y}(\boldsymbol{l})}$) dominates most of the energy transfer. However, as the system reaches the mid-quasi steady phase $t\omega_{ci} = 1045.6$ (right panel in Fig. 2), the inertial range narrows and $\overline{\partial S(\boldsymbol{l})/\partial t}$ takes over. A feature different from the turbulence case is that the sum of terms exhibits two plateaus, with the energy containing range sum larger than the inertial range value. Also, the structure function $S(l)$ does not show a clear $2/3$ slope, although it does exhibit a Kolmogorov-like $-5/3$ slope in the magnetic spectrum [36]. Note that it was previously shown [33, 36] that diffusion/exhaust/separatrix region (DES) and the island region make comparable contributions to $S(l)$.

To strengthen the characterization of a constant energy transfer rate in reconnection, in Fig. 3 we trace the time evolution of $\overline{\nabla_l \cdot \mathbf{Y}(\boldsymbol{l})}$ and $\overline{\partial S(\boldsymbol{l})/\partial t}$. As reconnection initiates, the MHD transfer term develops a full inertial range for $l > d_i$. The growth of $\overline{\partial S(\boldsymbol{l})/\partial t}$ lags behind the MHD transfer term and becomes significant only after the inertial range is fully populated; the time delay between the onset of these two terms is comparable to the delay (Fig. 3 (bottom)) between the onset of reconnection rate $d\Psi/dt$ (red), where Ψ is the magnetic flux and the increase in spectral energy density $E_B(k)$ at $kd_i \sim 1$ (dash-dot). The MHD transfer term continues to dominate the quasi-steady phase until about $t\omega_{ci} \approx 950$ when it changes sign.

In Fig. 3 (top) for large lags, the MHD transfer term oscillates in sign for a substantial period after reconnection onset. However these reversals are offset by an anti-correlated oscillation of the $\overline{\partial S(\boldsymbol{l})/\partial t}$ term (middle panel). These oscillations are certainly related to the well-known sign-indefinite character of insufficiently-averaged third-order correlators, as they can be removed by additional time-averaging (as in [57]). But there is
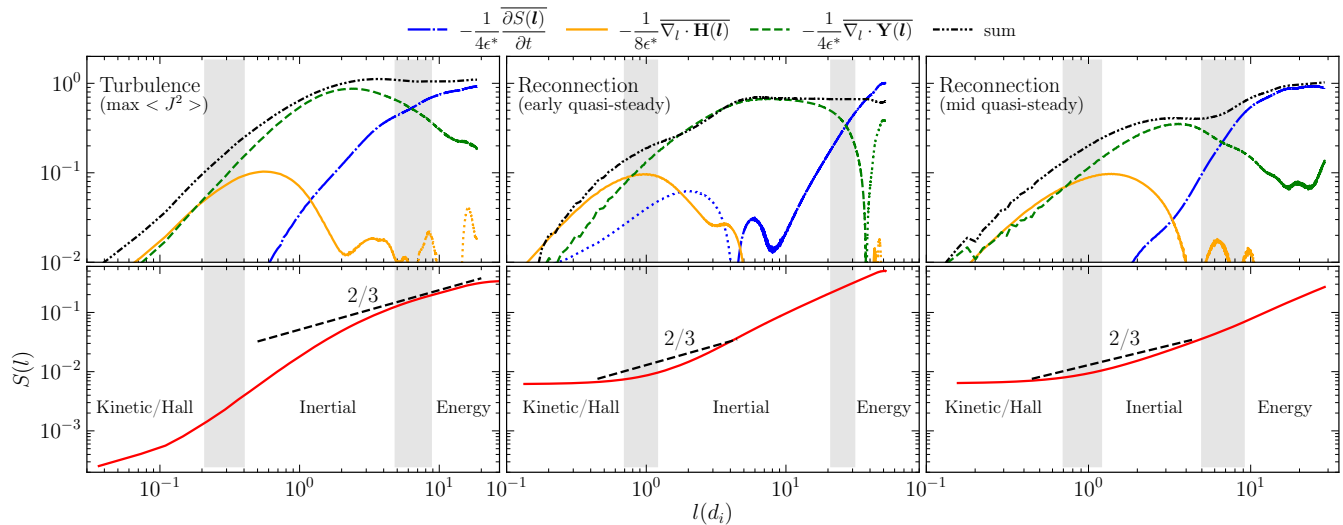
FIG. 2. Third-order law analysis for (left) turbulence simulation when rms current is peaked ($t\omega_{ci} = 163$), (middle) reconnection simulation during early quasi-steady phase ($t\omega_{ci} = 824.3$), and (right) reconnection simulation during mid quasi-steady phase ($t\omega_{ci} = 1045.6$). Top: Terms from the left hand side of Eq. 2 and their sum, normalized to ϵ^*. Bottom: Total second-order structure function $S(l)$ with a dashed line of slope 2/3 drawn for reference. Approximate regions of the energy containing range, inertial range, and kinetic/Hall range are separated by light gray vertical rectangles. When a given term is negative, the magnitude of the term is shown as a dotted curve with the same color.

TABLE II. Dissipation and energy transfer rate comparisons of simulations. Left to right: correlation scale λ; average dissipation rate ϵ^* during $\Delta t\omega_{ci}$ examined in Fig. 2; von Kármán energy dissipation rate using initial δZ; von Kármán constant C_{vk} (defined through $d(\delta Z^2)/dt = -C_{vk}\,\delta Z^3/\lambda \approx 2\,\epsilon^*$).

Run	$\lambda = \frac{1}{k_{av}}[d_i]$	$\epsilon^*[\frac{v_A^3}{d_i}]$	$\frac{\delta Z^3}{\lambda}[\frac{v_A^3}{d_i}]$	$C_{vk} = \frac{2\,\epsilon^*}{\frac{\delta Z^3}{\lambda}}$
A	8	1.7×10^{-4}	0.011	0.031
B	14.7	6.4×10^{-5}	0.006	0.021

also a tendency for 2.5D systems to inherit the large scale inverse transfer that occurs in a pure 2D MHD state [9, 59–61]. Large scale Alfvénic exchange between flow and magnetic energy, a familiar feature of MHD turbulence simulation corresponds to the observed oscillation period, which is roughly $90\,t\omega_{ci}$, about three times the global nonlinear time of the system $\tau_{nl} = L_{box}/(2\pi\,\delta Z) \approx 33\,\omega_{ci}^{-1}$.

Following the quasi-steady reconnection period ($t\,\omega_{ci} \gtrsim 1170$) in Fig. 3, the MHD scale energy transfer rate decreases as suggested by the reduction in both $\overline{\nabla_l \cdot \mathbf{Y}(l)}$ and $\partial S/\partial t$, as well as the decline of their sum for $l \approx 9\,d_i$. The correlation of MHD energy transfer (solid) and reconnection rate (dashed), evidenced by their near simultaneous decrease, indicates a strong connection between the two processes.

Conclusions: Using kinetic PIC simulations, we have cross-compared the behavior of the third-order law in

strong turbulence and laminar reconnection, which allows a direct measure of the energy transfer rate. We find a significant level of structural similarities in the lag dependence of the various terms of Eq. 2. Notably, both simulations exhibit an inertial range signified by a relatively constant and dominant MHD energy transfer term, a signature of a turbulent system. Both systems have an energy containing range wherein $\overline{\partial S(l)/\partial t}$ dominates and a kinetic range where the Hall term becomes important. These similarities provide evidence that the dynamics of reconnection proceeds through energy transfer similar to that seen in turbulence. Supporting this idea is the correlation between the reconnection rate, the sum of the MHD terms in Eq. 2, and the spectral energy density at $kd_i \sim 1$ observed in Fig. 3 (bottom).

A complimentary analysis of the reconnection and turbulence simulations is an estimate of the dissipation rate using the energy δZ^2 at the correlation scale λ; this estimate is based on the similarity decay theory of von Kármán and Howarth [62]. Table II gives the results of this analysis for the simulations and compares them to the dissipation rate ϵ^* and the MHD energy transfer rate ϵ. The von Kármán constant C_{vk} is the ratio of the actual energy dissipation to the estimated rate. While the turbulence simulation exhibits a C_{vk} similar to previous PIC turbulence simulations [63], the reconnection C_{vk} is about 2/3 of the turbulence value. This reduction is likely associated with the reconnection initial condition, having an energy-containing scale that is nearly at the maximum size permitted by the periodic box. This locks a fraction of the mean square magnetic potential in the
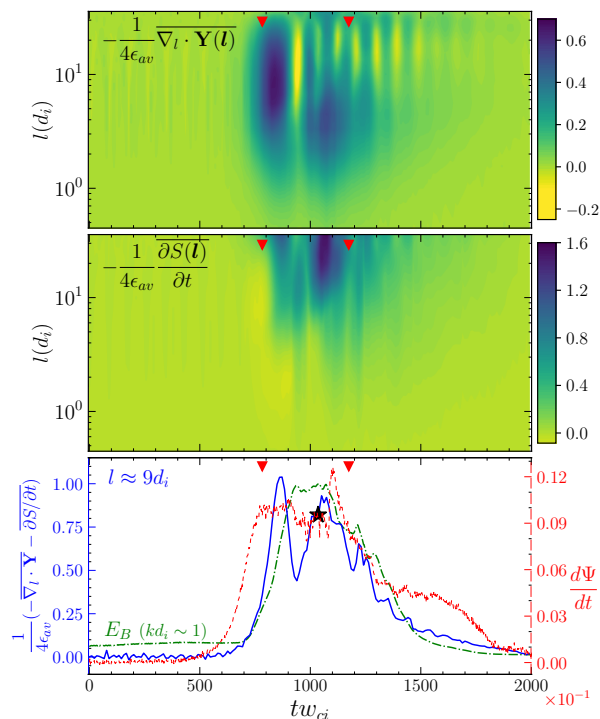
FIG. 3. Simulation B (reconnection): Time evolution of (top) $\overline{\nabla_l \cdot \mathbf{Y}(l)}$ and (middle) $\overline{\partial S(l)/\partial t}$ term, normalized to ϵ_{av}, the average rate of change of E_B plus E_{if} during the quasi-steady period of reconnection, denoted by red triangles. (Bottom) time variation of reconnection rate (dashed) and $\frac{-1}{4\epsilon_{av}}\left(\overline{\nabla_l \cdot \mathbf{Y}(l)} + \overline{\partial S(l)/\partial t}\right)$ at $l \approx 9\,d_i$ (solid), with the energy density $E_B(k)$ at $k\,d_i \sim 1$ (dash-dot). $E_B(k)$ is plotted with respect to the axis on the left and normalized to $(E_B(k))_{max}$. The black star denotes $d\Psi/dt$ at $t\omega_{ci} = 1045.6$.

largest scales, reducing the energy available to drive a direct transfer. This is the effect responsible for selective decay in 2D MHD [64] and is analogous to Taylor relaxation in 3D MHD. [65]. This weakens the transfer of energy in reconnection, but only fractionally.

We should also mention in passing that the energy transfer terms that we do include sum rather accurately to the total energy decay, scale by scale, supporting findings that MHD transfer is mainly local [66, 67], and with the majority of the transfer through incompressible channels (see fig. 2). We did find some suggestion of transient back-transfer (not shown here) to long wavelengths, which is a basic property of 2D MHD [64, 68], but we see no evidence for non-local pumping of small scales by large scales as suggested by [23].

On balance, the detailed study of reconnection from the perspective of energy transfer theory that we have presented here leads to what is perhaps a remarkable conclusion – that although one might not suspect that reconnection follows many of the assumptions of energy transfer theories such as the von Kármán Howarth equations for incompressible MHD, it exhibits energy transfer similar to that of standard turbulence. This does not diminish the importance of the special features of reconnection and especially its ramifications for kinetic physics. However, understanding that turbulence and reconnection are very closely related can only lead to a better understanding of each of these fundamental processes.

[1] P. J. Coleman Jr, The Astrophysical Journal **153**, 371 (1968).
[2] W. H. Matthaeus and M. L. Goldstein, Journal of Geophysical Research: Space Physics **87**, 6011 (1982).
[3] R. Bruno and V. Carbone, Living Reviews in Solar Physics **2**, 4 (2005).
[4] N. Banerjee and P. Sharma, Monthly Notices of the Royal Astronomical Society **443**, 687 (2014).
[5] L. Z. Hadid, F. Sahraoui, S. Galtier, and S. Huang, Physical review letters **120**, 055102 (2018).
[6] X. Shi, D. Nagai, H. Aung, and A. Wetzel, Monthly Notices of the Royal Astronomical Society **495**, 784 (2020).
[7] S. Servidio, W. Matthaeus, M. Shay, P. Cassak, and P. Dmitruk, Physical review letters **102**, 115003 (2009).
[8] M. Yamada, R. Kulsrud, and H. Ji, Reviews of Modern Physics **82**, 603 (2010).
[9] W. Matthaeus and S. L. Lamkin, The Physics of fluids **29**, 2513 (1986).
[10] H. Strauss, The Astrophysical Journal **326**, 412 (1988).
[11] S. Jabbari, A. Brandenburg, D. Mitra, N. Kleeorin, and I. Rogachevskii, Monthly Notices of the Royal Astronomical Society **459**, 4046 (2016).
[12] A. Lazarian, G. L. Eyink, A. Jafari, G. Kowal, H. Li, S. Xu, and E. T. Vishniac, Physics of Plasmas **27**, 012305 (2020).
[13] M. Zhou, N. F. Loureiro, and D. A. Uzdensky, Journal of Plasma Physics **86** (2020).
[14] N. Loureiro, D. Uzdensky, A. Schekochihin, S. Cowley, and T. Yousef, Monthly Notices of the Royal Astronomical Society: Letters **399**, L146 (2009).

[15] A. Beresnyak, The Astrophysical Journal **834**, 47 (2016).

[16] A. Beresnyak, Living Reviews in Computational Astrophysics **5**, 1 (2019).

[17] G. Eyink, E. Vishniac, C. Lalescu, H. Aluie, K. Kanov, K. Bürger, R. Burns, C. Meneveau, and A. Szalay, Nature **497**, 466 (2013).

[18] C. C. Lalescu, Y.-K. Shi, G. L. Eyink, T. D. Drivas, E. T. Vishniac, and A. Lazarian, Physical review letters **115**, 025001 (2015).

[19] F. Pucci, S. Servidio, L. Sorriso-Valvo, V. Olshevsky, W. Matthaeus, F. Malara, M. Goldman, D. Newman, and G. Lapenta, The Astrophysical Journal **841**, 60 (2017).

[20] P. Muñoz and J. Büchner, Physical Review E **98**, 043205 (2018).

[21] M. Wan, S. Oughton, S. Servidio, and W. Matthaeus, Physics of Plasmas **17**, 082308 (2010).

[22] C. C. Haggerty, T. N. Parashar, W. H. Matthaeus, M. A. Shay, Y. Yang, M. Wan, P. Wu, and S. Servidio, Physics of Plasmas **24**, 102308 (2017).

[23] E. Papini, L. Franci, S. Landi, A. Verdini, L. Matteini, and P. Hellinger, The Astrophysical Journal **870**, 52 (2019).

[24] J. Eastwood, T. Phan, S. Bale, and A. Tjulin, Physical review letters **102**, 035001 (2009).

[25] N. F. Loureiro and S. Boldyrev, Physical Review Letters **118**, 245101 (2017).

[26] S. Boldyrev and N. F. Loureiro, The Astrophysical Journal **844**, 125 (2017).

[27] L. Franci, S. S. Cerri, F. Califano, S. Landi, E. Papini, A. Verdini, L. Matteini, F. Jenko, and P. Hellinger, The Astrophysical Journal **850**, L16 (2017).

[28] G. Kowal, D. A. Falceta-Gonçalves, A. Lazarian, and E. T. Vishniac, The Astrophysical Journal **838**, 91 (2017).

[29] A. Mallet, A. A. Schekochihin, and B. D. Chandran, Journal of Plasma Physics **83** (2017).

[30] D. Vech, A. Mallet, K. G. Klein, and J. C. Kasper, The Astrophysical Journal Letters **855**, L27 (2018).

[31] R. Ergun, K. Goodrich, F. Wilder, N. Ahmadi, J. Holmes, S. Eriksson, J. Stawarz, R. Nakamura, K. Genestreti, M. Hesse, et al., Geophysical Research Letters **45**, 3338 (2018).

[32] E. Leonardis, S. C. Chapman, W. Daughton, V. Roytershteyn, and H. Karimabadi, Physical review letters **110**, 205002 (2013).

[33] F. Pucci, W. H. Matthaeus, A. Chasapis, S. Servidio, L. Sorriso-Valvo, V. Olshevsky, D. Newman, M. Goldman, and G. Lapenta, The Astrophysical Journal **867**, 10 (2018).

[34] G. Lapenta, F. Pucci, M. Goldman, and D. Newman, The Astrophysical Journal **888**, 104 (2020).

[35] G. Kowal, D. A. Falceta-Gonçalves, A. Lazarian, and E. T. Vishniac, The Astrophysical Journal **892**, 50 (2020).

[36] S. Adhikari, M. Shay, T. Parashar, P. S. Pyakurel, W. Matthaeus, D. Godzieba, J. Stawarz, J. Eastwood, and J. Dahlin, Physics of Plasmas **27**, 042305 (2020).

[37] H. Politano and A. Pouquet, Physical Review E **57**, R21 (1998).

[38] P. Hellinger, A. Verdini, S. Landi, L. Franci, and L. Matteini, The Astrophysical Journal Letters **857**, L19 (2018).

[39] N. Andrés, F. Sahraoui, S. Galtier, L. Z. Hadid, P. Dmitruk, and P. D. Mininni, Journal of Plasma Physics **84** (2018).

[40] S. Banerjee and N. Andrés, Physical Review E **101**, 043212 (2020).

[41] V. Carbone, R. Marino, L. Sorriso-Valvo, A. Noullez, and R. Bruno, Physical review letters **103**, 061102 (2009).

[42] D. Biskamp, Magnetohydrodynamic turbulence (Cambridge University Press, 2003).

[43] R. Bruno and V. Carbone, Living Reviews in Solar Physics **10**, 1 (2013).

[44] T. N. Parashar, W. H. Matthaeus, and M. A. Shay, The Astrophysical Journal Letters **864**, L21 (2018).

[45] Y. Yang, W. H. Matthaeus, Y. Shi, M. Wan, and S. Chen, Physics of Fluids **29**, 035105 (2017).

[46] W. H. Matthaeus, Y. Yang, M. Wan, T. N. Parashar, R. Bandyopadhyay, A. r. Chasapis, O. Pezzi, and F. Valentini, apj **891**, 101 (2020).

[47] A. N. Kolmogorov, C.R. Acad. Sci. U.R.S.S. **32**, 16 (1941), [Reprinted in Proc. R. Soc. London, Ser. A **434**, 15–17 (1991)].

[48] U. Frisch, Turbulence: The Legacy of AN Kolmogorov (Cambridge University Press, 1995).

[49] A. Verdini, R. Grappin, P. Hellinger, S. Landi, and W. C. Müller, The Astrophysical Journal **804**, 119 (2015).

[50] R. Ferrand, S. Galtier, F. Sahraoui, R. Meyrand, N. Andrés, and S. Banerjee, The Astrophysical Journal **881**, 50 (2019).

[51] R. Bandyopadhyay, L. Sorriso-Valvo, A. Chasapis, P. Hellinger, W. H. Matthaeus, A. Verdini, S. Landi, L. Franci, L. Matteini, B. L. Giles, et al., Physical Review Letters **124**, 225101 (2020).

[52] A. Monin and A. Yaglom, Statistical Fluid Mechanics: Mechanics of Turbulence, Vol. II (Dover Publications, Inc., 1975).

[53] W. H. Matthaeus, Y. Yang, M. Wan, T. N. Parashar, R. Bandyopadhyay, A. Chasapis, O. Pezzi, and F. Valentini, The Astrophysical Journal **891**, 101 (2020).

[54] H. Aluie and G. L. Eyink, Physical review letters **104**, 081101 (2010).

[55] S. Banerjee and S. Galtier, Phys. Rev. E **87**, 013019 (2013), 10.1103/PhysRevE.87.013019.

[56] P. Hellinger, E. Papini, A. Verdini, S. Landi, L. Franci, L. Matteini, and V. Montagud-Camps, The Astrophysical Journal **917**, 101 (2021).

[57] M. A. Taylor, S. Kurien, and G. L. Eyink, Physical Review E **68**, 026310 (2003).

[58] A. N. Kolmogorov, Proceedings of the Royal Society of London. Series A: Mathematical and Physical Sciences **434**, 9 (1991).

[59] W. Matthaeus and D. Montgomery, Annals of the New York Academy of Sciences **357**, 203 (1980).

[60] A. Alexakis, Phys. Rev. E **84**, 056330 (2011).

[61] J. T. Coburn, M. A. Forman, C. W. Smith, B. J. Vasquez, and J. E. Stawarz, Philosophical Transactions of the Royal Society A: Mathematical, Physical and Engineering Sciences **373**, 20140150 (2015).

[62] T. De Karman and L. Howarth, Proceedings of the Royal Society of London. Series A-Mathematical and Physical Sciences **164**, 192 (1938).

[63] P. Wu, M. Wan, W. Matthaeus, M. Shay, and M. Swisdak, Physical review letters **111**, 121105 (2013).

[64] W. H. Matthaeus and D. Montgomery, Annals of the New York Academy of Sciences **357**, 203 (1980).

[65] J. B. Taylor, Phys. Rev. Lett. **33**, 1139 (1974).

[66] M. K. Verma, A. Ayyer, and A. V. Chandra, Physics of Plasmas **12**, 082307 (2005), 10.1063/1.1993067.

[67] H. Aluie and G. L. Eyink, Phys. Rev. Lett. **104**, 081101 (2010), 10.1103/PhysRevLett.104.081101.

[68] D. Fyfe, D. Montgomery, and G. Joyce, J. Plasma Phys. **17**, 369 (1977).

[69] Computational and Information Systems Laboratory, "Cheyenne: HPE/SGI ICE XA System (University Community Computing)," (2017).